

4 Shenghua Jiang, Fang Liu, Min-Gyu Kim, Jae-Hong Lim, Kun-Jae Lee, Yong-Ho
5 Choa, Kyung Song, Michael J. Sadowsky, Wilfred Chen, Nosang V. Myung*, and
6 Hor-Gil Hur*

*To whom correspondence should be addressed: Hor-Gil Hur (Tel: +82-062-970-2437; Fax: +82-062-970-2434; E-mail: hghur@gist.ac.kr). Nosang V. Myung (Tel: +1-951-827-7710; Fax: +1-951-827-5696; E-mail: myung@engr.ucr.edu)

11 **Materials and Methods**

12 **Formation of ternary As-S-Se and As-Cd-S, and quaternary As-Cd-S-Se**
13 **nanotubes**

14 The As-S nanotubes were produced by *Shewanella* sp. HN-41 in the dark at 30°C
15 for 7 days as previously described¹. The nanotubes were collected from culture
16 medium, washed three times in anaerobic deionized water, and then injected into the
17 the HEPES-buffered basal medium² which supplemented with 10 mM sodium lactate
18 as the electron donor and 2 mM sodium selenite as the electron acceptor to produce
19 the ternary As-S-Se nanotubes. Inoculation of bacteria was performed in the same way
20 as producing As-S, followed by incubation in the dark at 30°C for 24 hr. In contrast,
21 the ternary As-Cd-S nanotubes were produced through an abiotic galvanic
22 displacement reaction. The As-S nanotubes were washed in anaerobic deionized water
23 for 3 times, followed by resuspending in N₂-purged 2 mM CdCl₂ solution. The
24 reaction was performed under the dark at 30°C with gently shaking for 2 hr. The
25 quaternary As-Cd-S-Se nanotubes were biologically synthesized by using the purified
26 As-Cd-S nanotubes as the precursor under the same conditions as used for the
27 synthesis of the ternary As-S-Se nanotubes.

28 The samples were collected at selected time during the microbial and abiotic
29 reactions for the detection of arsenic, sulfide, selenite and Cd(II) in the aqueous
30 reaction solutions. Culture supernatants were filtered through a 0.2 µm membrane
31 filter (MFS-25, Advantec MFS, Inc., Dublin, CA), and the filtrates were diluted and
32 acidified with 2% HNO₃ for analysis using inductively-coupled plasma mass
33 spectrometry (ICP-MS, Agilent Technologies 7500ce, Palo Alto, CA). The
34 concentration of sulfide in aqueous phase was determined by the methylene blue
35 method³.

36

37 **Material characterization**

38 The morphology of the nanotubes was examined by using scanning and
39 transmission, and high resolution transmission electron microscope (SEM, TEM, and
40 HR-TEM). SEM and TEM images were obtained using a Hitachi S-4700 FE-SEM
41 (Tokyo, Japan) and Jeol JEM-2100F (Tokyo, Japan), respectively. SAED (selected
42 area electron diffraction) and FFT (Fast Fourier Transform) analyses were conducted
43 using the HR-TEM to determine crystal structures and grain size. Spatial resolved
44 elemental analyses of cross sections of the nanotubes were done by using FE-TEM in
45 Korea Basic Science Institute (KBSI, Daejeon, Korea). The crystal structure of the
46 nanotubes was investigated by using X-ray diffraction (XRD, D/MAX Uitima III,
47 Rigaku, Tokyo, Japan).

48 For XAS, the x-ray absorption spectra were recorded at the BL7C (EC) beamline
49 of a Pohang light source (Pohang Accelerator Laboratory, Pohang, Republic of Korea)
50 with a Si(111) monochromator and a ring current of 120-170 mA at 2.5 GeV. Spectra
51 were collected in fluorescence mode for all samples. The reference compounds used
52 for this analysis were as follows: As₂S₃ and As₂Se₃ powder (Acros Organics, Geel,
53 Belgium), Cd powder, CdS, CdSe, selenium powder [Se(0)], sodium selenite [Se(IV)],
54 and copper selenide [Se(-2)] (Aldrich, St. Louis, MO).

55

56 **Electrical characterization**

57 Electrode arrays were microfabricated as described previously⁴ on silicon
58 substrate using standard lithographic patterning. Approximately 100 nm thick SiO₂
59 film was first deposited on a highly doped p-type (100) oriented Si wafer using
60 thermal chemical vapor deposition (CVD) to insulate the substrate. The electrode area

61 was defined by photolithography using positive photoresist, followed by e-beam
62 evaporation of a 200 Å-thick Cr adhesion layer and a ~1800 Å-thick gold layer.

63 Finally, electrodes (200 μm × 200 μm) separated by a gap of approximately 3 μm
64 were defined using lift-off techniques.

65 To fabricate nanotubes network interconnects across the electrodes; first,
66 synthesized nanotubes were dispersed in deionized water. Then, a 3 μl drop of the
67 nanotubes suspension solution was manually dispensed on top of the electrode gap
68 using a micro syringe, followed by applying AC dielectrophoretic field of $V_{rms} = 0.36$
69 V at $f = 4$ MHz. After assembly, the devices were rinsed with deionized water, dried
70 by gently blowing of nitrogen gas. To reduce the contact resistance between the
71 electrodes and nanotubes, the samples were annealed at 100°C for 10 min in ambient
72 environments. The temperature dependent current-voltage (I-V) characteristics were
73 measured using a single-channel system source meter instrument (Keithley, Model
74 236, Cleveland, OH) with various of temperature from 40 to 270 K using cold-finger
75 cryogenic system (Janis CCS-350SH). Activation energies (E_A) were calculated from
76 electrical resistance Arrhenius plots in the temperature region above 210 K. The
77 field-effect transistor transfer characteristics were measured by using the highly doped
78 Si substrate as a back gate. The electrical measurements were performed using a
79 dual-channel system sourcemeter instrument (Keithley 2636, Cleveland, OH) in
80 ambient environments and at room temperature.

81

82 **Supplementary Description**

83 The As-S nanotubes were produced by *Shewanella* sp. HN-41 in the dark at 30°C
84 for 7 days as previously described¹. The purified bright yellow As-S nanotubes were
85 resuspended in the same medium supplemented with 10 mM lactate and 2 mM

86 sodium selenite as the electron donor and acceptor, respectively. Inoculation of
87 bacteria was performed in the same way as producing As-S. The products were
88 composed of filamentous structures and the average diameter was approximately
89 48 ± 14 nm (ESI Fig. S1b) similar to the precursor As-S nanotubes (ESI Fig. S1a). The
90 XRD pattern of the nanotubes showed a broad peak with no distinct peaks, indicating
91 that the nanotubes were amorphous (ESI Fig. S3a) similar to the precursor As-S
92 nanotubes.

93 The As-Cd-S nanotubes were synthesized through an abiotic process. The
94 purified As-S nanotubes, which were formed previously in 100 ml medium, were
95 resuspended in the same volume containing 2 mM CdCl₂. As the reaction time
96 increased, the color of the bright yellow As-S nanotubes changed to jacinthe. The
97 average diameter of the filamentous was 46 ± 13 nm (ESI Fig. S1c) close to that of the
98 As-S nanotubes. XRD spectral analysis showed several diffraction peaks of CdS with
99 the preferred crystal orientation in the (444) and (107) direction (ESI Fig. S3b).
100 Although the As-S phase was not observed in the XRD pattern of the As-Cd-S
101 nanotubes, As₂S₃ phase in the nanotubes was observed in FFT (ESI Fig. S4b) analysis,
102 indicating that a small amount of As₂S₃ co-existed with CdS in the As-Cd-S
103 nanotubes. Similar to Se anionic exchange process, Cd K-edge XANES characterization for the
104 As-Cd-S nanotube directly presents successful ion-exchange reaction between host arsenic and
105 guest cadmium ions (ESI Fig. S5b).

106 As-Cd-S was purified and resuspended in the same medium containing bacteria
107 and 2 mM Se(IV) as described above. The average diameter of the filamentous was
108 47 ± 13 nm similar to that of the As-Cd-S nanotubes (ESI Fig. S1d). XRD spectra
109 showed several diffraction peaks assigned to CdS with no peaks corresponding to
110 CdSe and AsSe (ESI Fig. S3c). The preferred crystal planes of CdS in the As-Cd-S-Se
111 nanotubes were (444) and (107) which is similar to the As-Cd-S nanotubes. On the

112 other hand, CdSe was observed with CdS and As₂S₃ in the FFT analysis (ESI Fig.
113 S4d) of the As-Cd-S-Se nanotubes. These results suggest that maybe only trace
114 amount of Se replaced S and bonded to Cd. The Cd and Se K-edge XANES after
115 dual-ion exchange only showed a Se-As chemical interaction without any Se-Cd
116 chemical bonding, whereas those for the Cd ion directly present distinct Cd-S
117 chemical interaction and an absence of Cd-Se bonding (ESI Fig. S5c). The fact
118 indicated that after the first Cd cationic exchange, the second Se anionic exchange can
119 be occurred in not Cd site but only arsenic site. As a result, there coexist arsenic
120 sulfide, cadmium sulfide and arsenic selenide phases in the As-Cd-S-Se nanotube.

121 ESI Fig. S6, S7, and S8 show the electrical properties of the As-S, As-S-Se, and
122 As-Cd-S-Se nanotubes, respectively. The carrier concentration and field effect
123 mobility were estimated using following equations:

124
$$p = C_G V_{G,T} / e L_{SD}$$
 Eq. (2)

125
$$\mu = L_{SD}^2 dI / dV / C_G V_D$$
 Eq. (3)

126
$$C_G = \epsilon W L_{SD} / L_{OX}$$
 Eq. (4)

127 where p is the hole carrier concentration, C_G the approximate capacitance, $V_{G,T}$
128 the threshold voltage to deplete the nanotubes, μ the field effect carrier mobility,
129 V_D the drain voltage, and ϵ the dielectric constant of SiO₂. The transconductance
130 of dI/dV was taken from each transfer characteristics in the linear regime to
131 calculate the field effect mobility of μ . As shown in the Figure 4c, the source-drain
132 current (I_{DS}) was strongly dependent on the gate bias where a clear off-state was
133 observed at positive bias voltage. These results infer that the As-Cd-S nanotubes are
134 p-type semiconductor with the carrier concentration and field effect mobility of
135 $1.1 \pm 0.4 \times 10^{10} \text{ cm}^{-3}$ and $0.08 \pm 0.01 \text{ cm}^2/\text{Vs}$, respectively (ESI Fig. S9b).

136 Supporting Information Figures S8a and b show comparison of grain size,
137 thermal activation energy, carrier concentration, and field effect mobility among the
138 As-S, As-Cd-S, As-Se-S and Cd-As-Se-S nanotubes. The conduction of the nanotubes
139 was governed by the grain boundary scattering where the amorphous/nanocrystalline
140 As-S and As-S-Se nanotubes have much lower carrier concentration and mobility than
141 the single or polycrystalline As-Cd-S and As-Cd-Se-S nanotubes. As expected, we
142 found that the nanocrystalline As-Cd-S and As-Cd-Se-S nanotubes have lower thermal
143 activation energy, E_A , than the amorphous As-S and As-Se-S nanotubes (ESI Fig.
144 S9a).

145 If interface states and bound charges at gate dielectric/nanotubes are absent, the
146 concentration of the carriers and field effect mobility are mainly controlled by
147 structure of the nanotubes and the superposition of gate electric field. Even though the
148 carrier concentration of all nanotubes is around 10^{10} cm^{-1} , the field effect mobility was
149 strongly depended on the composition of the nanotubes. For example, the quaternary
150 As-Cd-S-Se nanotubes show highest field effect mobility, indicating that it has lowest
151 interface states among them (ESI Fig. S9b). These results revealed that the
152 incorporation of Cd and/or Se into the As-S nanotubes could tune both structural and
153 electrical properties.

154

155 **Supplementary Figures**

156

157 Fig. S1. Size distributions of As-S (a), As-S-Se (b), As-Cd-S (c), and As-Cd-S-Se (d)
158 nanotubes. Numbers of the nanotubes counted, averages and standard deviations of
159 the diameters of the nanotubes are shown on the diagrams. Solid lines: Estimation by
160 Gaussian fitting.

161

162 Fig. S2. TEM image with EDX line profile across the cross section of the As-S-Se
163 nanotube (a), and tubular structure observed by low-resolution TEM image (arrowed)
164 (b).

165

166 Fig. S3. X-ray diffraction patterns of As-S-Se (a), As-Cd-S (b) and As-Cd-S-Se (c)
167 nanotubes.

168

169 Fig. S4. HR-TEM image (a) and FFT with the analyzed compositions (b) for the
170 As-Cd-S nanotubes, and HR-TEM image (c) and FFT with the analyzed compositions
171 (d) for the As-Cd-S-Se nanotubes.

172

173 Fig. S5. Normalized Se K-edge XANES spectra for the As-S-Se (a), As-Cd-S (b), and
174 As-Cd-S-Se nanotubes (c).

175

176 Fig. S6. Electrical characteristics of the As-S nanotubes. Temperature dependent I-V
177 curves (a), resistance change as a function of temperature (b), and transfer
178 characteristics of As-S nanotubes with inset SEM image of aligned As-S nanotubes
179 between electrode pads (scale bar: 1 μ m) (c).

180

181 Fig. S7. Electrical characteristics of the As-S-Se nanotubes. Temperature dependent
182 I-V curves (a), resistance change as a function of temperature (b), and transfer
183 characteristics of As-S-Se nanotubes with inset SEM image of aligned As-S-Se
184 nanotubes between electrode pads (scale bar: 1 μ m) (c).

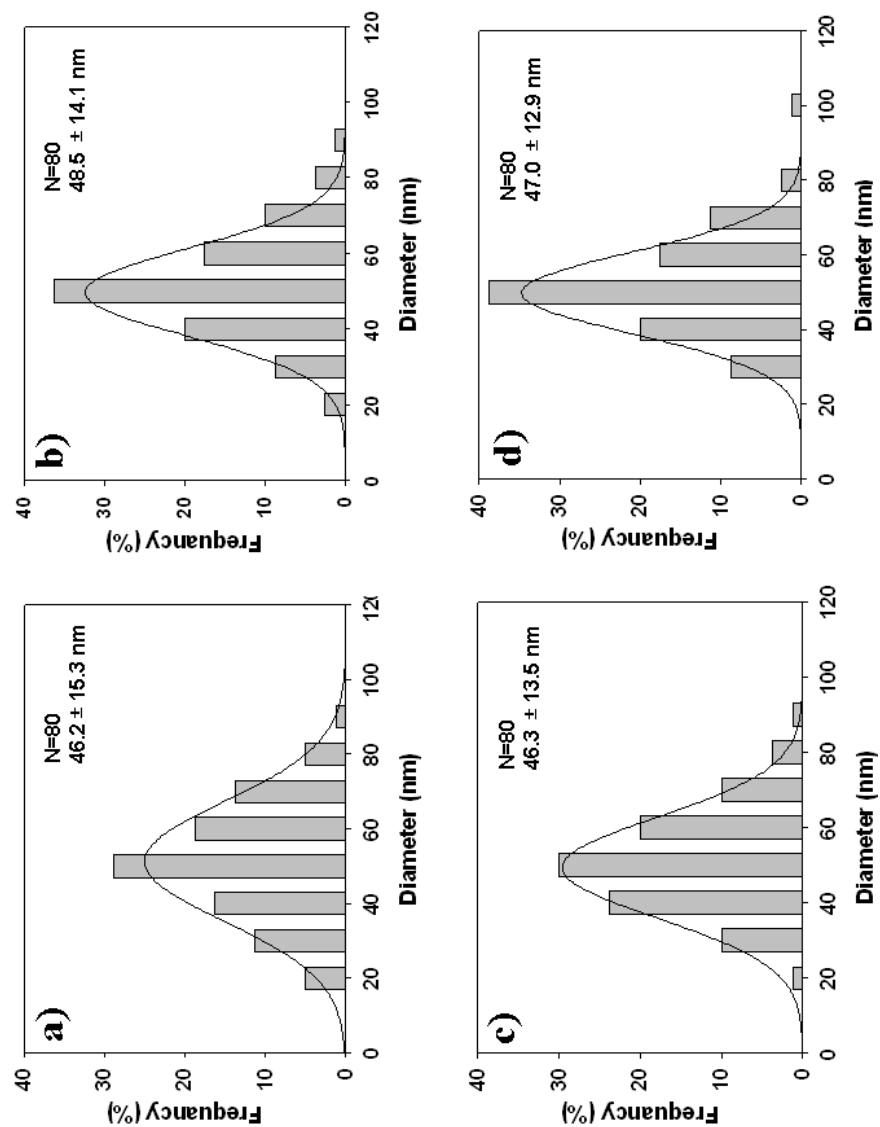
185

186 Fig.S8. Electrical characteristics of the As-Cd-S-Se nanotubes. Temperature
187 dependent I-V curves (a), resistance change as a function of temperature (b), and
188 transfer characteristics of As-Cd-S-Se nanotubes with inset SEM image of aligned
189 As-Cd-S-Se nanotubes between electrode pads (scale bar: 1 μ m)(c).

190

191 Fig. S9. Grain size vs. thermal activation energy (a) and field effect mobility vs.
192 carrier concentration of As-S, As-Cd-S, As-S-Se, and As-Cd-S-Se nanotubes (b).

Fig. S1.



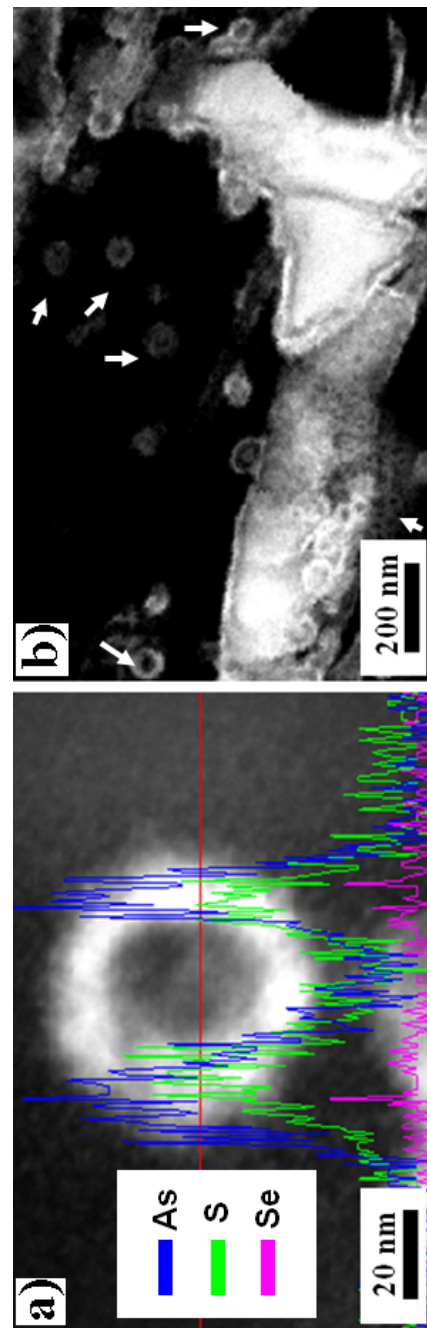
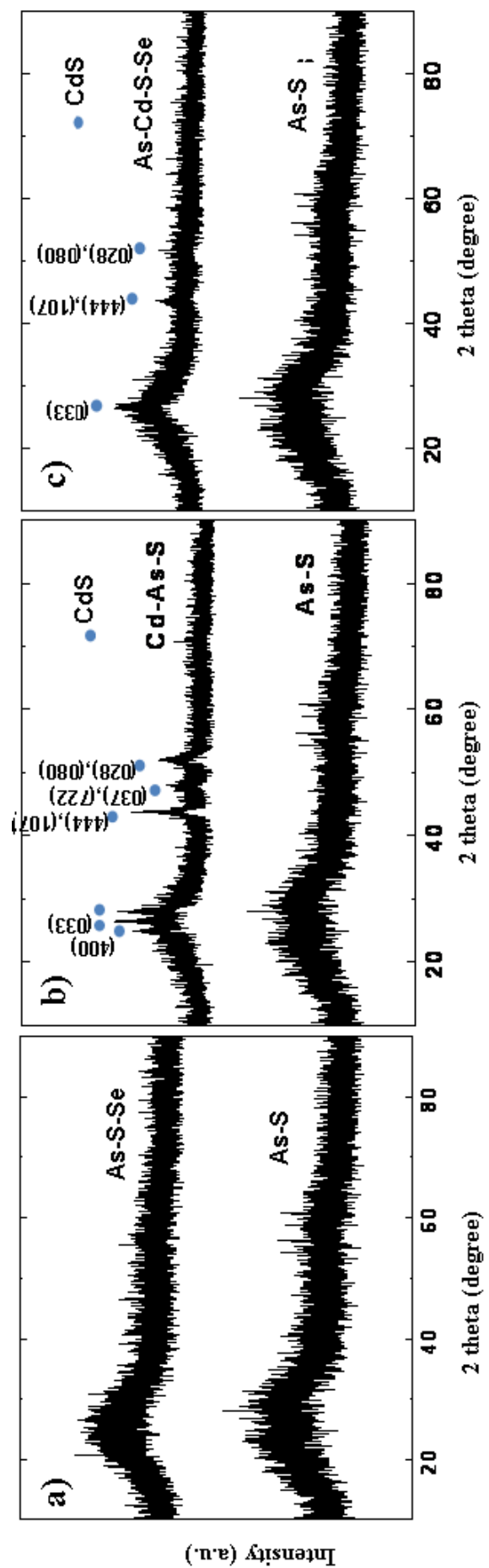


Fig. S2.

Fig. S3.



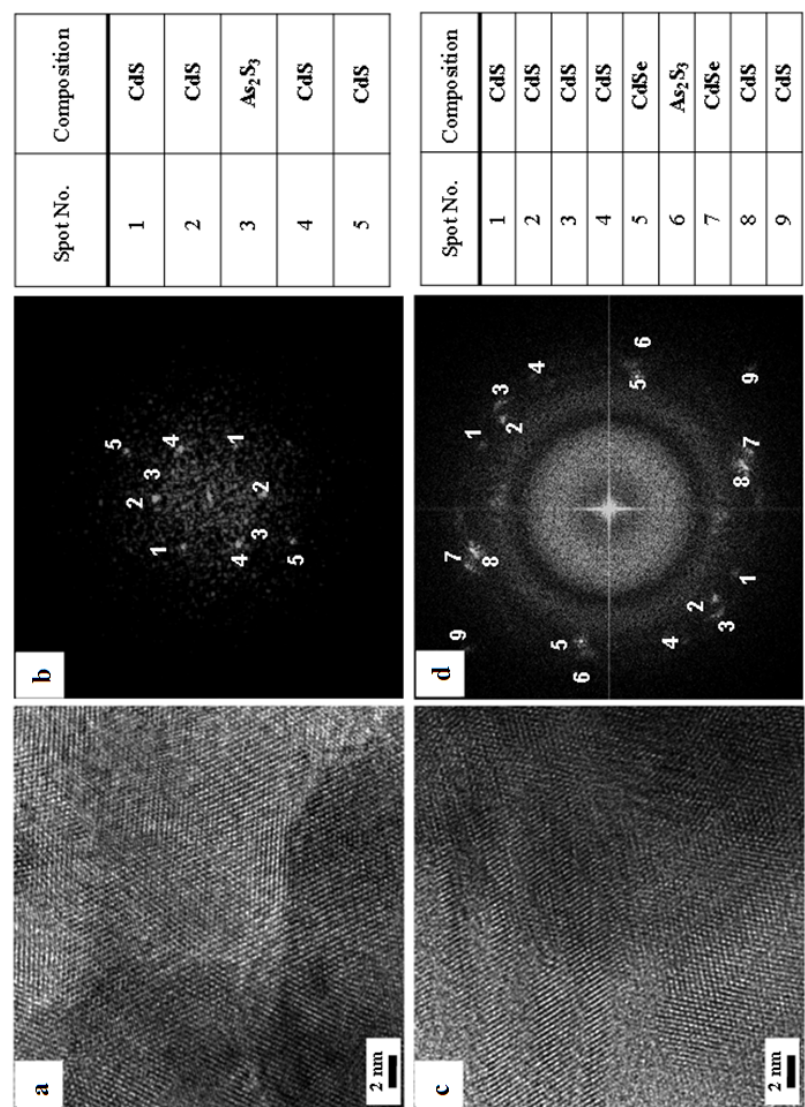


Fig. S4.

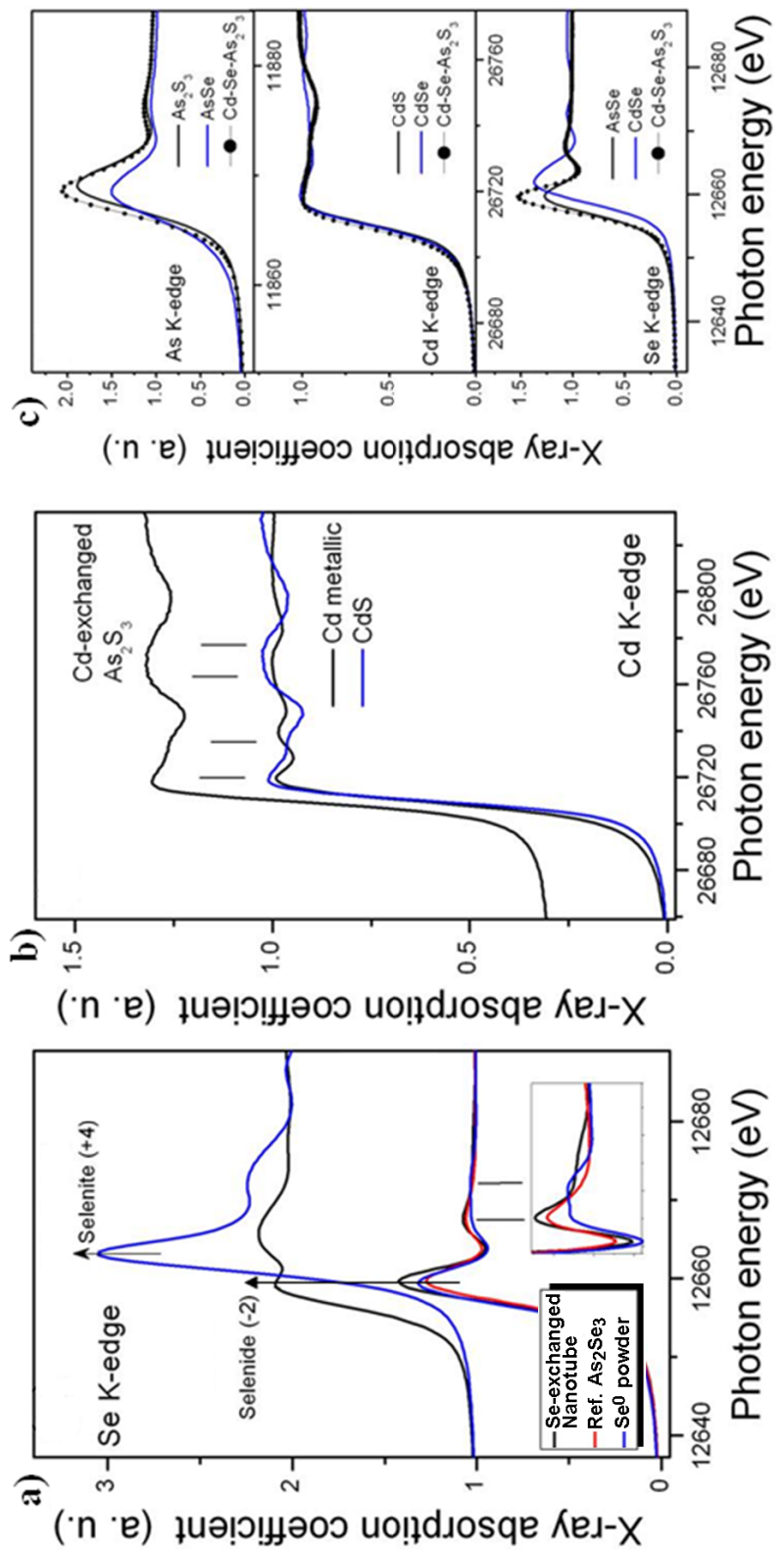


Fig. S5.

Fig. S6.

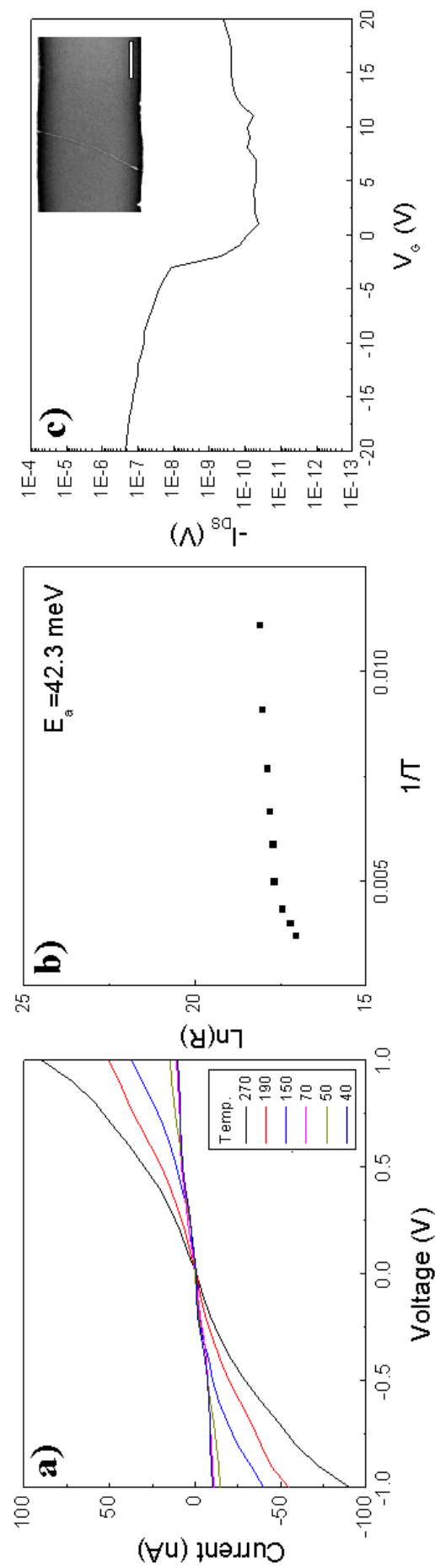


Fig. S7.

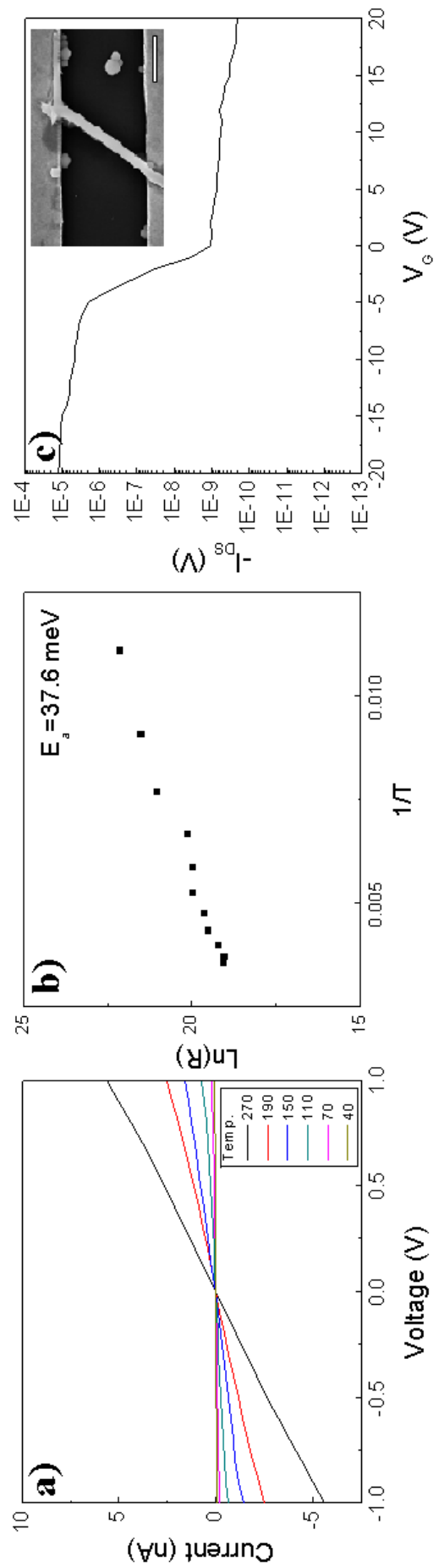


Fig. S8.

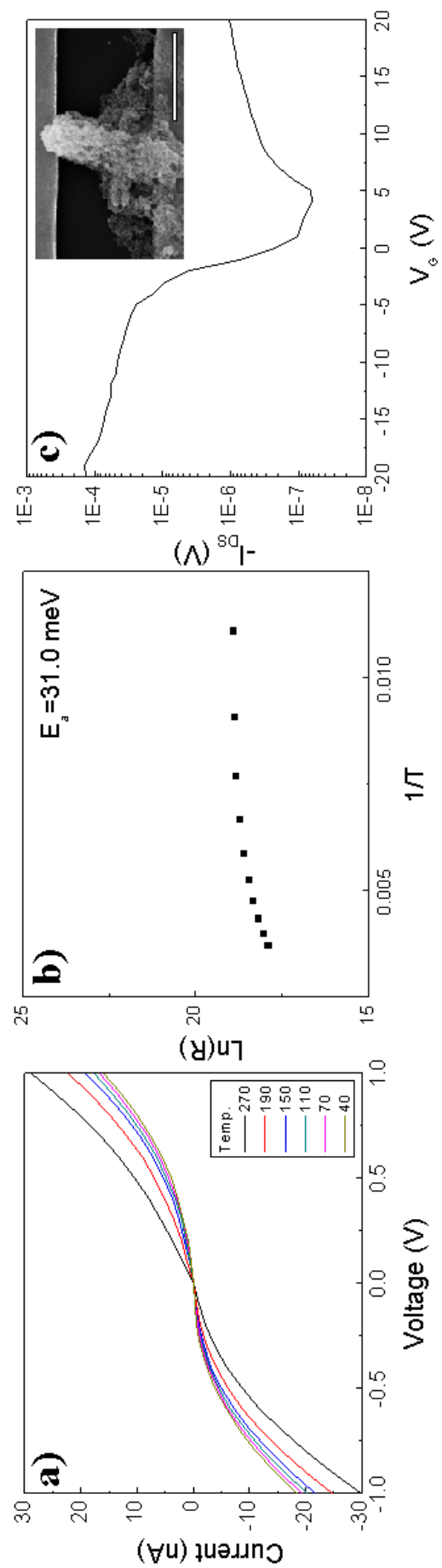
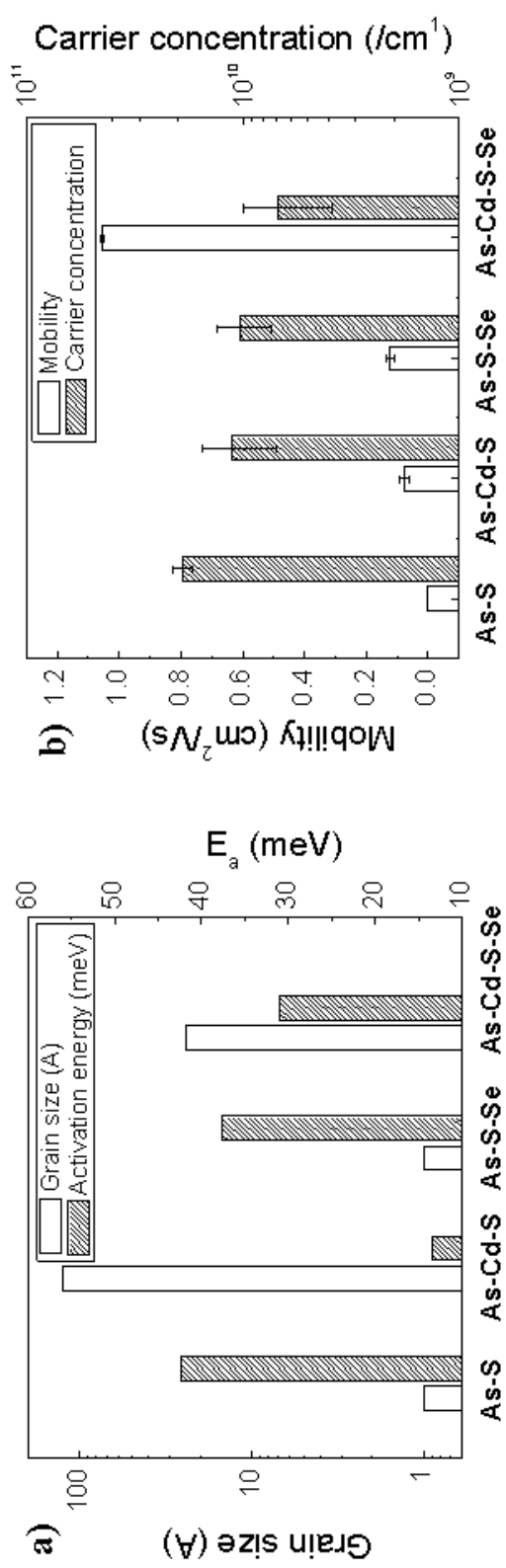


Fig. S9.



Reference

1. J.-H. Lee, M.-G. Kim, B. Yoo, N. V. Myung, J. Maeng, T. Lee, A. C. Dohnalkova, J. K. Fredrickson, M. J. Sadowsky and H.-G. Hur, *Proc. Natl. Acad. Sci. USA*, 2007, **104**, 20410-20415.
2. J. H. Lee, Y. Roh, K. W. Kim and H.-G. Hur, *Geomicrobiol. J.*, 2007, **24**, 31-41.
3. J. K. Fogo and M. Popowski, *Anal. Biochem.*, 1949, **21**, 732-734.
4. S. Mubeen, T. Zhang, B. Yoo, M. A. Deshusses and N. V. Myung, *J. Phys. Chem. C.*, 2007, **111**, 6321-6327.
5. M. Popescu, F. Sava, N. Aldea, X. Yaning, H. Tiandou, L. Tao and M. Leonovici, *Chalcogen. Lett.*, 2005, **2**, 71-76.